Int J Thermophys (2010) 31:2305–2322
DOI 10.1007/s10765-010-0882-x

Determination of the Effusivity of Different Scratched Coaxial Temperature Sensors Under Hypersonic Flow

H. A. Mohammed · H. Salleh · M. Z. Yusoff

Received: 25 November 2009 / Accepted: 10 November 2010 / Published online: 1 December 2010

Abstract This paper presents an experimental method for determining the effusivity values of different scratched coaxial temperature sensors. These sensors have a response time on the order of microseconds (50 μs) with a rise time of less than 0.3 μs. Two types of scratch were used, mainly abrasive papers with different grit sizes and scalpel blades with different thicknesses to form the sensor junctions. The effect of the scratch technique on the sensor's effusivity is also investigated. The sensors were tested and calibrated in the test section of a shock-tube facility at different operating conditions. It was observed that the effusivity of a particular sensor depends on the Mach number, scratch technique, scratch direction, junction location, as well as on the enthalpy condition. It was also noticed that a scratched sensor using the scalpel blade technique does not require an individual calibration. However, for a sensor scratched using the abrasive paper technique, a calibration for each sensor is likely to be required. The present results have provided useful and practical data of the effusivity values for different scratched temperature sensors. These data are beneficial to experimentalists in the field, and can be used for accurate transient heat transfer rate measurements.

Keywords Coaxial temperature sensors · Effusivity · Scratched technique · Shock tube · Transient heat flux

1 Introduction

Temperature is one of the fundamental thermodynamic properties and several engineering applications frequently require measuring the temperature variation of

H. A. Mohammed (✉) · H. Salleh · M. Z. Yusoff
Department of Mechanical Engineering, College of Engineering, Universiti Tenaga Nasional, Km 7, Jalan Kajang-Puchong, 43009 Kajang, Selangor, Malaysia
e-mail: hussein@uniten.edu.my

surfaces exposed to a fast changing heat flux. Typical examples of surfaces experiencing rapid temperature fluctuations include internal combustion engine cylinder walls [1–6], aerodynamics facilities [7–9], gun barrels [10], and in boiling experiments [11–13]. In order to measure a fast transient surface temperature in a short-time duration flow (few microseconds), and to indicate the true surface temperature of a component, the need of a temperature sensor having a fast response time is necessary. The coaxial sensor design was originally proposed by Bendersky [14], which consisted of a small wire coated with 12 μm aluminum oxide insulation and securely inserted in a tube. Other surface probes have been fabricated using scratches from abrasive paper or a sharp implement [15]. In addition, the surface probes have been manufactured using two parallel wires [16] or ribbon elements [1–3] that are insulated from each other except at the exposed surface. The coaxial temperature sensor offers distinct advantages as follows: (i) low cost compared with a commercial sensor [17]; (ii) its sensing surface can be refurbished if broken during the experiment; (iii) fast response time (less than 50 μs); (iv) stable and repeatable in dynamic calibration experiments; and (v) easy to be contoured to any model surface (cone, cylinder, sphere, etc.) due to its small size and sturdy design.

All temperature sensors used in this work were fabricated in-house, and their construction details are reported in [18]; therefore, an individual dynamic calibration for each particular temperature sensor is required for accurate results. This is also to acquire an accurate and single value of its effusivity (β). This will consequently be used in the calculation of the transient heat flux by the inverse heat conduction method. Additionally, the calibration of each temperature sensor is also essential because there will be errors of up to 23 % or even higher [18] if the thermophysical properties of the sensor materials are obtained from the literature [19–21]. Many investigators have measured the effusivity using different techniques. Alkidas and Cole [2] calibrated heat flux probes using a water-cooled, high intensity radiation source with 36 kW, and with a reference heat flux sensor. A radiative technique with a laser pulse was used by Gatowski et al. [4] to measure the value of (β) for several types of surface-temperature probes. However, this technique requires a lamp of the calibrated intensity, a value for the absorbtivity of the assembled probe surface, and a relatively long exposure time (on the order of 100 ms) to achieve useful surface-temperature changes. The same technique was employed by Buttsworth [22] using a tungsten–halogen lamp to provide a step heat flux input to an eroding ribbon Type K commercial probe [17] for relatively long time scales, from about 0.1 s to 1 s. This may lead to an inappropriate value of β if the time scales of interest are much shorter than can be assessed with this calibration technique. Kovács and Mesler [15] utilized a 200 J flash tube as a high intensity transient heat source. However, it is difficult to determine the appropriate β at short-time scales (around 50 μs) using this technique. This is because this technique leads to erroneous values of β due to two main factors: (i) the absorbtivity of the probe surface cannot be accurately predicted for short-time scale calibration and furthermore, (ii) the exposure time is much longer than the intended application of the probes. The laser pulse technique was proposed by Heichal et al. [23] to assess the dynamic performance of a surface probe by measuring its unit-impulse response function (UIRF). Sprinks [24] presented a numerical technique to determine the thermal capacitance of a calorimeter gauge using a plunging technique. However, this technique is not

preferable as it requires a knowledge of the thermophysical properties of the fluid, and measurements of both the initial bath temperature and the gauge temperature during the plunging process. Lyons and Gai [25] described a method for determining the effusivity (β) for a thin film or surface probe at a given temperature rise using an optical technique with a known power laser. Although this technique was shown to be quick and versatile, it is costly and requires special equipment; thus, it is undesirable. Gai and Joe [8] and Sanderson and Sturtevant [9] calibrated surface probes in a free piston driven shock tunnel to measure the heat transfer rate on a spherically blunted cone and circular cylinder. However, they did not identify the appropriate effusivity values for the probes tested.

From the above literature review, the prior work has investigated the insulation influence [15,22], but they did not clearly identify the importance of the various sensor materials including the thermophysical property differences between the positive and negative sensor elements. Furthermore, they did not also identify the effusivity values for different sensors with different sensing surfaces for microsecond time scales. Thus, in this paper an experimental method for identifying the effective effusivity values for miniature, reliable, fast response temperature sensors is described. The performance of these sensors in a shock-tube facility is also discussed. The effect of using different scratch types, mainly abrasive paper and scalpel blade, on the sensors' effusivity values is also investigated.

2 Sensor Construction

2.1 Fabrication Technique

A short summary of the construction steps of the temperature sensor is given below (see, for more details, Ref. [18]). The current design and fabrication approach depend mainly on the thermoelectric emf produced at a junction of dissimilar metals. This work uses the sensor material itself as the substrate to produce a particularly robust design and able to tolerate a large transient heat flux. The temperature sensor was designed and fabricated from Type K elements (alumel/chromel). It consists of a 1 mm inner wire with one element positive or negative and a hollow machined annulus 2 mm from the other element either positive or negative having a thickness of 0.25 mm. The preparation of the inner wire and the outer annulus was done by using a wire cutting machine, and the annulus was drilled using a drill bit with a very fine thickness. The inner wire was then placed symmetrically and coaxially into a hollow machined cylinder of the other element.

The sensor junction was fabricated by abrading its exposed surface to create a burr across the small gap. In this case very fine tolerances are required to produce a small gap between the sensor elements, and the effective thickness of the junction scales with the width of the gap. Thus, the sensor junctions were formed by gently sanding its end surface using two different scratch techniques: (i) abrasive paper with different grit sizes; (ii) scalpel blade with different thicknesses. The abrasive papers have the following grit sizes: 100#, 150#, 200#, 320#, 400#, 600#, 800#, 1000#, 1200#, 1500#, and 2000# (Shandong Boss Abrasives Manufacturing Co. Ltd., China). The scalpel

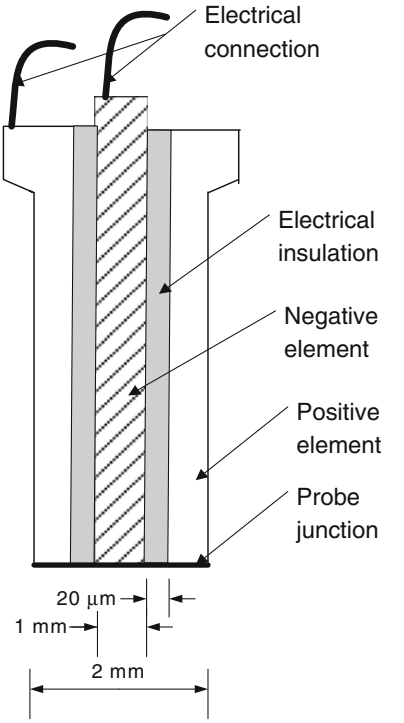

Fig. 1 Schematic diagram of temperature sensor assembly

blades have the following thicknesses: 20 μm, 40 μm, and 60 μm (Yancheng Huida Medical Instruments Co. Ltd., China). In addition, the sensor elements were insulated by a very thin layer of epoxy 'Araldite' having a thickness of a few micrometers. A schematic diagram of the final temperature sensor assembly is shown in Fig. 1. The retained parameters of sensors when passing from one sample to another are the length and diameter of the sensor elements, and these parameters were carefully controlled in the manufacturing process by accurate measurements of the length and diameter of the two elements. In addition, the use of a single type of abrasive paper or scalpel blade is carried out by moving the abrasive paper with a particular grit size at the end of the assembly in two horizontal directions (i.e., back and forth). The movement of the abrasive paper should be continued until the surface of the assembly becomes smooth and plain. However, one perpendicular direction of cut was used for the scalpel blade scratch technique to form the junction. The testing results of the temperature sensors indicate that a successful sensor could be made even with an electrical insulation with an average thickness of 20 μm. However, it is determined that the probability of a successful sensor construction will be enhanced if the thickness of the gap can be decreased. Although the surface junction of the temperature sensor is formed through direct mechanical contact between the two elements, the temperature sensor has been successfully shown to be quite robust (response time less than 50 μs) in a harsh environment (e.g., shock tube) as can be seen in the next sections.

2.2 Sensors Thermophysical Properties

One of the objectives of this work is to accurately measure the time-varying surface heat flux using the fabricated temperature sensor. Thus, there is a need to know the thermophysical properties of the substrate or more precisely the value of the effusivity (β). Therefore, new correlation equations to evaluate the thermophysical properties for temperature sensor elements are developed in order to have another means to determine the thermophysical properties consistently with a high level of accuracy.

The selection of thermophysical properties of temperature sensor elements was taken from Caldwell [26] and Touloukian [27,28]. However, according to Caldwell [26], the approximate analysis of Type K temperature sensor elements are as follows: (i) alumel constituents are: (94 % to 96 %) Ni, (1 % to 1.5 %) Si, (1.3 % to 2.5 %) Al, (1.8 % to 3.25 %) Mn, and iron and other constituents in smaller quantities and (ii) chromel constituents are: (89 % to 90 %) Ni, (9 % to 9.5 %) Cr, up to 0.5 % Si, (0.02 % to 0.65 %) Fe, and (0.01 % to 0.8 %) Mn. Although nickel is the major constituent of Type K elements, there are significant differences in the thermophysical properties of the chromel and alumel materials. Furthermore, according to Touloukian [27], the alumel consists of 72 % Ni, 25 % Mn, 2 % Al, 1 % Si, and the chromel is the same as Caldwell's composition (i.e., 90 % Ni, 10 % Cr). As has been highlighted by the same authors [18], the values of β for both alumel and chromel elements differ from each other by about 23 % at 25 °C and also differ from the mean value by about 15 % at ambient temperature. Conclusively, a dynamic calibration for each particular temperature sensor is required for accurate results. Therefore, the data were collected again from Caldwell [26] and Touloukian [27,28]. New correlation equations are developed for the specific heat (c) and thermal conductivity (κ) of both elements and presented as functions of temperature in Figs. 2 and 3. These straight-line correlations are typically obtained by identifying the slope from the data in Touloukian [27,28] and the intercept from the data reported in Caldwell [26]. This approach is most obvious from the alumel specific-heat correlation (Fig. 2) where the closest material composition reported in Touloukian [27] (72 % Ni, 1 % Si, 2 % Al, and 25 % Mn) differs significantly from the alumel analysis reported by Caldwell [26]. Thus, the following correlation equations are obtained:

For the chromel element:

$$c_{\mathrm{Cr}} = 0.178664T + 375.053 \tag{1}$$

$$\kappa_{\mathrm{Cr}} = 0.0191119T + 11.8513 \tag{2}$$

and for the alumel element:

$$c_{\mathrm{Al}} = 0.0751194T + 452.678 \tag{3}$$

$$\kappa_{\mathrm{Al}} = 0.0298301T + 17.9676 \tag{4}$$

In addition, the values of β for both alumel and chromel elements, based on the developed correlation equations (Eqs.1–4) and the reported densities, can easily be calculated as a function of temperature. At 20 °C, $\beta_{\mathrm{Cr}} = 8\,070\,\mathrm{J \cdot m^{-2} \cdot K^{-1} \cdot s^{-1/2}}$

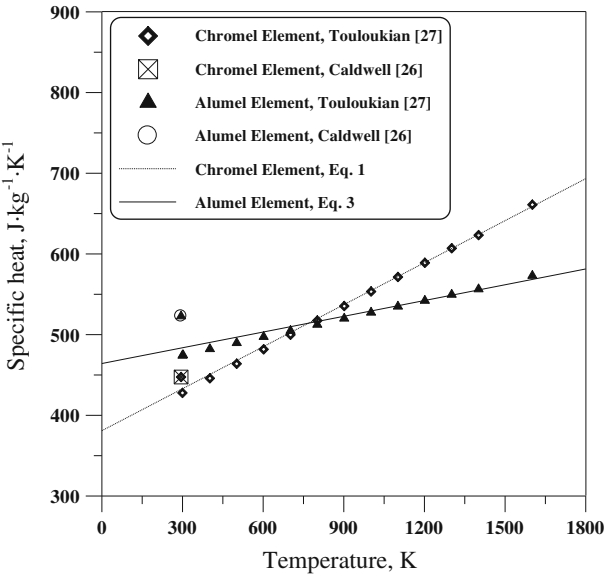

Fig. 2 Specific heat versus temperature for temperature sensor elements

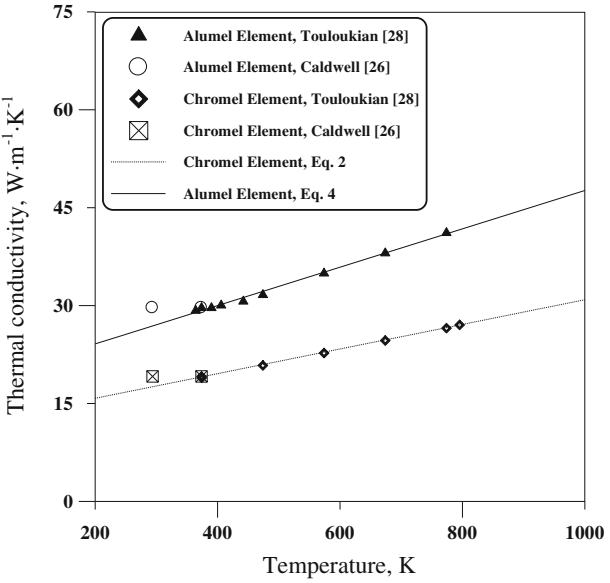

Fig. 3 Thermal conductivity versus temperature for temperature sensor elements

and $\beta_{\mathrm{Al}} = 10\,442\,\mathrm{J}\cdot\mathrm{m}^{-2}\cdot\mathrm{K}^{-1}\cdot\mathrm{s}^{-1/2}$ which amounts to a difference of 2 372 $\mathrm{J}\cdot\mathrm{m}^{-2}\cdot\mathrm{K}^{-1}\cdot\mathrm{s}^{-1/2}$ or around 23 %. Thus, a dynamic calibration for each temperature sensor is required as the effective value of the effusivity for a particular temperature sensor construction depends upon the junction location, whether it is located on the

chromel or alumel elements, and its location relative to the electrical insulation, as will be demonstrated in Sect. 5.

3 Experimental Setup

The dynamic calibrations of the fabricated temperature sensors were performed in a UNITEN shock-tube facility to determine its response time and to confirm its capability for measuring the transient surface temperature and consequently establishing the transient heat flux. A full description of this facility is reported in [18]. A brief description of the shock-tube setup and its instrumentation is given below. The layout of a UNITEN shock-tube facility is illustrated in Fig. 4. The facility consists of a driver section; flange, wherein the diaphragm is placed; driven section; connection piece; working section (test section); and end-cap wall. The driver and driven sections are made of stainless steel (304L grade), designed to withstand 20 MPa pressure. They are 2.5 m and 4.25 m in length, respectively, with 0.09 m outside diameter and 0.05 m inside diameter for each. The diaphragm, a thin instantaneously removable diaphragm aluminum sheet of 0.2 mm thickness, is placed in the flange between the driver and driven sections until the compression process is initiated. These diaphragms will burst if subjected to a pressure difference of (2 ± 0.07) MPa.

At the downstream end of the driven section, a 0.5 m length, 0.05 m inner diameter, and 0.09 m outer diameter stainless steel tube is called the "test section." It is interconnected with the driven section using a connection piece of 0.15 m length and 0.13 m diameter. This test section is used to calibrate the measuring instrumentation, including the constructed temperature sensors. Successful temperature sensors with different forms of scratched junctions were installed and glued into bushings at different axial locations along the test section. The test section temperature sensors were aligned with the inner surface of the driven sections to within approximately 0.1 mm, so that their sensing point was approximately flash mounted with the inner surface of the test section.

The driver and driven sections of the shock tube are equipped with a pressure gauge with a pressure range up to 16 MPa with an uncertainty of 70 kPa, to monitor the fill pressure inside the driver or driven sections. A vacuum pressure gauge with an accuracy of (0.2 ± 0.07) MPa is also installed in the driver and driven sections together

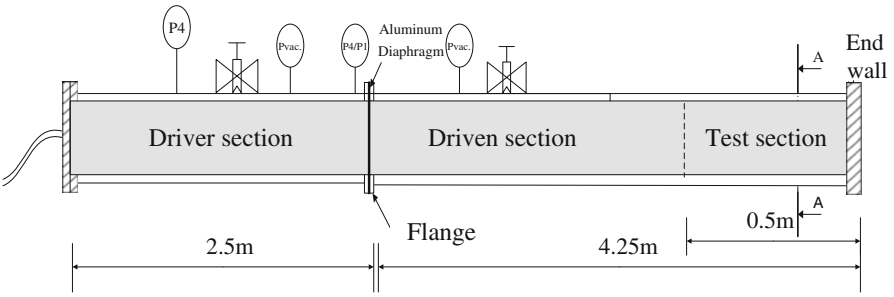

Fig. 4 Shock-tube facility configuration

with a vacuum pump to regulate the gas inside the driver or driven sections at different pressure values ranging from 0.1 MPa to (0.025 ± 0.07) MPa. The vacuum pump was used when the gas inside the driver or driven sections is not air (e.g., helium or CO_2); then the driver or driven sections should be evacuated and refilled with the required gas. There is also a piezoresistive static pressure transducer with a maximum pressure of 25 MPa with an uncertainty of 0.3 %. It is located at the end of the driver section and near the diaphragm position (flange) to monitor the exact diaphragm burst pressure history when the shock wave is propagated through the tube.

In this work, a test section with its end-cap wall was designed and manufactured with different axial and radial distances as shown in Fig. 5a, b. This test section contains nine drilled holes with 20 mm diameter and 20 mm depth. Seven of them were located in the upper part of the test section to sense and measure the transient surface-temperature rise within the test section's wall using the fabricated temperature sensor. Another two holes were located in the lower part of the section for measuring the

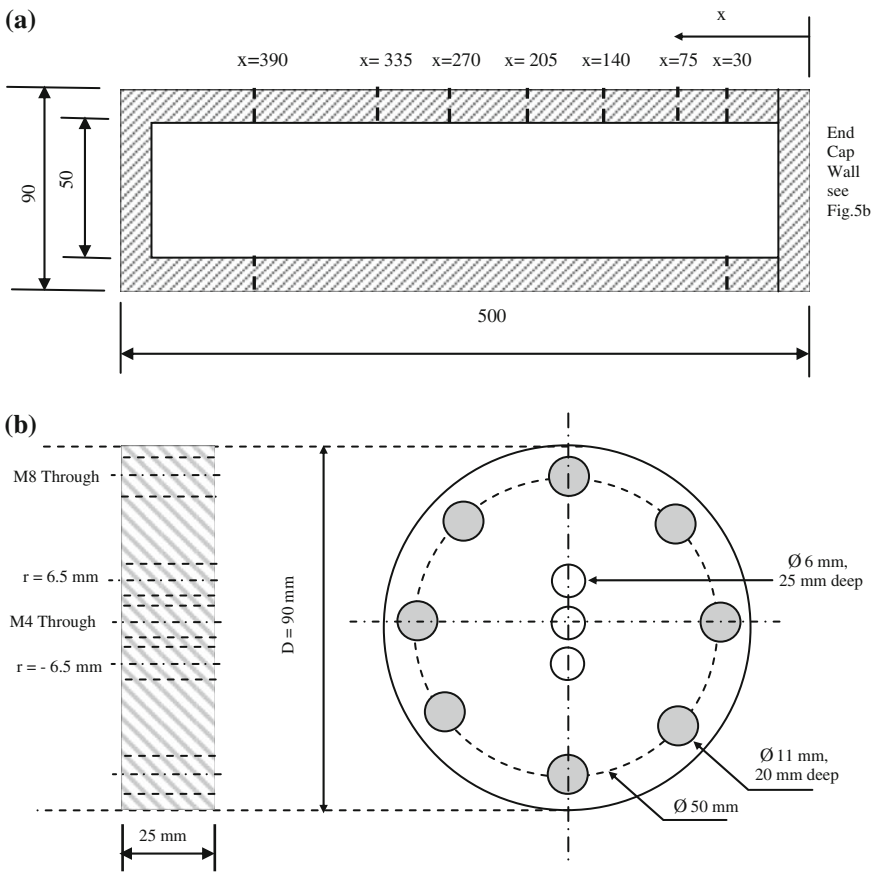

Fig. 5 (a) Shock-tube test section arrangement showing the locations of the measuring instrumentation, all dimensions are in mm and (b) Shock-tube end cap wall arrangement

pressure history data from the two piezoelectric pressure transducers (PCB Piezotronics Inc., Model 111A24) with 70 MPa maximum pressure with an uncertainty of 0.2 %, which were flush-mounted with the tube inner surface and it is precisely separated by 360 mm. The pressure transducers were also used to measure the shock-wave speed and to determine the precise time that the shock wave passed over the temperature sensor.

4 Method for Determining Effusivity of Sensors

In this work, the method of determining β is performed by calibrating all in-house fabricated temperature sensors using the shock-tube facility at microsecond time scales. Therefore, the following calibration equation is employed as suggested by Jessen et al. [7]:

$$\frac{T_{\mathrm{TS}} - T_{\infty}}{T_{\mathrm{R5}} - T_{\infty}} = \frac{\beta_{\mathrm{R5}}}{\beta_{\mathrm{R5}} + \beta_{\mathrm{TS}}} \tag{5}$$

where T_{R5} and β_{R5} are the temperature and effusivity of the working fluid behind the reflected shock wave. $T_{\mathrm{TS}} - T_{\infty}$ is the surface-temperature rise measured by the fabricated temperature sensor, and β_{TS} is the effusivity for a particular temperature sensor which can be determined from Eq. 5. This equation was used to evaluate the value of β for each temperature sensor with sufficient precision, the departure from the recorded surface temperature, and the temperature step in the working fluid during the shock reflection process at the end wall of the test section tube.

The working fluid temperature change $T_{\mathrm{R5}} - T_{\infty}$ was evaluated from the incident shock wave speed (u) using a calorically imperfect, ideal-gas analysis. The density (ρ_5), pressure (P_5), and the enthalpy (h_5) of the working fluid behind the reflected shock wave were also calculated from the ideal-gas equations as given by Anderson [29] and Zurcow and Hoffman [30]. The thermal conductivity of the working fluid was estimated using Sutherland's law given by White [31],

$$\frac{\kappa}{\kappa_{\mathrm{o}}} = \left(\frac{T_{\mathrm{R5}}}{T_{\mathrm{o}}}\right)^{\frac{3}{2}} \frac{T_{\mathrm{o}} + S}{T_{\mathrm{R5}} + S} \tag{6}$$

where κ_{o} and T_{o} are the thermal conductivity and the temperature of the working fluid at reference conditions, respectively, and S is the Sunderland constant.

The constant-pressure specific heat of the ideal gas was calculated using the following equation given by Vargaftik et al. [32]:

$$c_p = R\left(\sum_{j=0}^{6} \alpha_j \theta^j + \sum_{j=1}^{6} \beta_j \theta^{-j}\right) \tag{7}$$

where α and β are constants, $\theta = T_{\mathrm{R5}}/100$, R is the universal gas constant, and T_{R5} is the temperature behind the reflected shock wave.

5 Results and Discussion

A total of 80 test runs were carried out using 16 fabricated temperature sensors constructed using different scratch techniques (details are presented in Table 1). The experiments were conducted using a helium–CO_2 combination in the shock-tube facility with different diaphragm pressure ratios (P_4/P_1) ranging from 10 to 200. Figure 6 shows the designations of the fabricated temperature sensors used in this work. The value of the effusivity for each individual temperature sensor is predicted by measuring the true surface temperature.

5.1 Surface-Temperature Rise

Examples of the transient surface-temperature rise produced by the current temperature sensor formed with different scratch techniques are shown in Fig. 7 for selected test runs. This figure obviously shows that there is a small change in the surface-temperature rise. This is due to the difference between the effusivity of the working fluid

Table 1 Temperature sensors fabrication details

Temperature sensor no.	Scratch technique	Grit size no./scalpel blade thickness	Method of forming the junction	Junction location	Insulation thickness (μm)
KP80A	Abrasive paper	80#	Chromel to alumel	Alumel (A)	20
KP80A/R*	Abrasive paper	80#	Chromel to alumel	Alumel (A)	18
KP150C	Abrasive paper	150#	Alumel to chromel	Chromel (C)	16.4
KP150C/R*	Abrasive paper	150#	Alumel to chromel	Chromel (C)	15
KP320AC/K**	Abrasive paper	320#	Chromel to alumel	Alumel and chromel (AC)	15
KP400A	Abrasive paper	400#	Chromel to alumel	Alumel (A)	17
KP600AC/K**	Abrasive paper	600#	Chromel to alumel	Alumel and chromel (AC)	16
KP1000AC/K**	Abrasive paper	1000#	Chromel to alumel	Alumel and chromel (AC)	19.4
KP1200AC	Abrasive paper	1200#	Chromel to alumel	Alumel and chromel (AC)	14
KP1500AC/K**	Abrasive paper	1500#	Chromel to alumel	Alumel and chromel (AC)	18
KS20A	Scalpel blade	20 μm	Chromel to alumel	Alumel (A)	18.8
KS20C	Scalpel blade	20 μm	Alumel to chromel	Chromel (C)	18
KS40C	Scalpel blade	40 μm	Alumel to chromel	Chromel (C)	17.4
KS40C	Scalpel blade	40 μm	Alumel to chromel	Chromel (C)	16.6
KS60A	Scalpel blade	60 μm	Chromel to alumel	Alumel (A)	16.9
KS60C	Scalpel blade	60 μm	Alumel to chromel	Chromel (C)	18.8

P stands for abrasive paper; *A* stands for alumel element; *C* stands for chromel element; *AC* stands for both alumel and chromel elements; *K* stands for temperature sensor Type K; *R** means the fabrication of a particular temperature sensor is repeated; ** means that this particular temperature sensor is re-refurbished; and *S* stands for scalpel blade

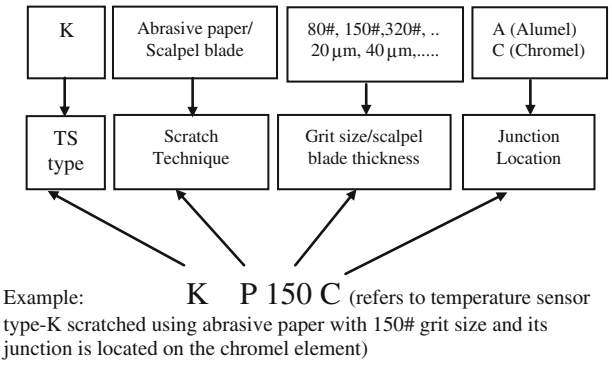

Fig. 6 Designation of the fabricated temperature sensor

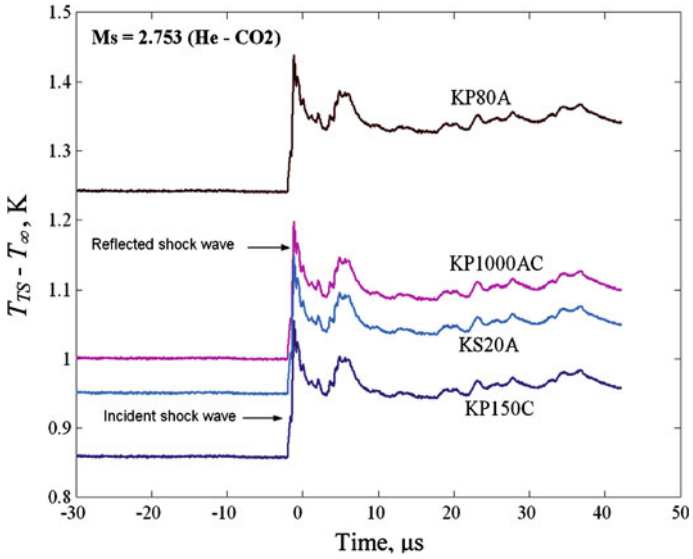

Fig. 7 Surface-temperature-rise history measured by different temperature sensors at $M_s = 2.753$

(CO_2 in this case) compared with that of the temperature sensor, even though there is a large change in CO_2 temperature due to shock-wave compression. Furthermore, there is ideally no movement of CO_2 in contact with the temperature sensor immediately following the shock reflection. Thus, CO_2 remains stationary for only a short period of time following the shock reflection due to the boundary-layer jetting effect which affects CO_2 at the end of the shock tube. Figure 7 also shows that there are two main peaks in the surface-temperature-rise history. The first peak reveals the propagation of the incident shock wave which compresses and heats the CO_2 to a higher temperature as indicated in the figure. The second peak refers to the reflected shock-wave propagation which is again compressed and heated the CO_2 to a higher temperature. Then, the surface temperature starts eventually to be uniform after the strength of the incident shock wave and reflected shock wave become weak. For example, the

Table 2 Temperature sensor testing conditions used in shock-tube facility with helium–CO_2 combination

Run no.	Incident Mach number (M_s)	Enthalpy $\left(\mathrm{kJ \cdot kg^{-1}}\right)$	T_{R5} (K)	$\beta_{R5}\left(\mathrm{J \cdot m^{-2} \cdot K^{-1} \cdot s^{-1/2}}\right)$
1	2.211	244.945282	703.7657	9.7029331
2	2.753	398.384242	959.9344	14.265216
3	3.371	604.063687	1317.035	19.952868
4	4.057	870.781971	1796.055	26.564816
5	4.289	970.154467	1977.857	28.819012
6	5.035	1321.18592	2630.497	39.456455

surface temperature for temperature sensor KP150C was increased in the first peak to 0.92 K, whereas it was increased to 1.02 K in the second peak. Furthermore, Fig. 7 illustrates that the surface-temperature rise value differs slightly for each temperature sensor. This depends on the method of forming the junction, the junction location on the positive/negative element, and its location relative to the insulation layer. This will be further investigated and interpreted in the next sections.

The experimental dynamic calibration conditions are presented in Table 2, and the experimental results are tabulated in Table 3 using the shock-tube facility for the helium–CO_2 combination. Six test runs from low enthalpy to high enthalpy were carried out to assess the temperature sensor performance and to evaluate the appropriate effusivity for each individual temperature sensor. It was observed from the testing in the shock-tube facility that there was a noisy response from the following sensors, KP400A, KP1200AC, KS20C, and KS40C, as they are short circuited. This is probably happened due to the imperfect contact between the sensor elements and also due to the lack of electrical insulation between these elements. Thus, these sensors need to be re-fabricated.

5.2 Effusivity Values

The effusivity values produced from the experimental dynamic calibration results are plotted and depicted in Figs. 8 and 9. It can be seen that the effusivity (β_{TS}) for each particular temperature sensor is a function of the calibration conditions (temperature of the working fluid and the enthalpy). Thus, it is revealed that the variability (standard deviation of the mean values) of the fabricated temperature sensors differs from one to another as they depend on the scratch technique used and on the junction location. It is also noticed from the helium–CO_2 experiments that there is variability in the fabricated temperature sensors. However, the scratched temperature sensors using abrasive paper and scalpel blade show close variability except for KP600AC and KS20A whose variability are 10.02 % and 10.26 %, respectively. The variability for KP80A is 4.54 %, for KP150C is 2.31 %, for KP320AC is 9.61 %, for KP1000AC is 8.92 %, for KP1500AC is 8.39 %, for KS40C is 4.19 %, for KS60A is 1.02 %, and for KS60C is 1.41 %. In the analysis of each test run, the recorded step surface temperatures using

Table 3 Temperature sensor experimental testing results using shock tube facility with helium-CO_2 combination

Run no.	Temperature sensor no.	Scratch technique	$T_{TS} - T_{\infty}$ (K)	β_{TS} $\left(J \cdot m^{-2} \cdot K^{-1} \cdot s^{-1/2}\right)$
1	KP80A	Abrasive paper 80#	0.351	11309.493
	KP150C	Abrasive paper 150#	0.41	9683.426
	KP320AC	Abrasive paper 320#	0.422	9408.35
	KP600AC	Abrasive paper 600#	0.395	10050.79
	KP1000AC	Abrasive paper 1000#	0.367	10816.859
	KP1500AC	Abrasive paper 1500#	0.358	11088.55
	KS20A	Scalpel blade 20 μm	0.382	10392.50
	KS40C	Scalpel blade 40 μm	0.448	8862.89
2	KP80A	Abrasive paper 80#	0.941	10094.43
	KP150C	Abrasive paper 150#	0.978	9713.08
	KP320AC	Abrasive paper 320#	0.91	10437.818
	KP600AC	Abrasive paper 600#	0.821	11567.777
	KP1000AC	Abrasive paper 1000#	0.872	10892.06
	KP1500AC	Abrasive paper 1500#	0.894	10624.37
	KS20A	Scalpel blade 20 μm	0.933	10180.86
	KS40C	Scalpel blade 40 μm	1.02	9313.71
3	KP80A	Abrasive paper 80#	1.971	10366.34
	KP150C	Abrasive paper 150#	2.245	9103.485
	KP320AC	Abrasive paper 320#	1.59	12845.444
	KP600AC	Abrasive paper 600#	1.692	12072.28
	KP1000AC	Abrasive paper 1000#	1.626	12561.49
	KP1500AC	Abrasive paper 1500#	1.64	12454.43
	KS20A	Scalpel blade 20 μm	2.376	8602.68
	KS40C	Scalpel blade 40 μm	1.85	11042.95
4	KP80A	Abrasive paper 80#	3.816	10476.05
	KP150C	Abrasive paper 150#	4.194	9534.26
	KP320AC	Abrasive paper 320#	3.357	11904.8
	KP600AC	Abrasive paper 600#	3.127	12778.48
	KP1000AC	Abrasive paper 1000#	3.964	10085.91
	KP1500AC	Abrasive paper 1500#	4.271	9362.85
	KS60A	Scalpel blade 60 μm	3.551	11255.87
	KS60C	Scalpel blade 60 μm	4.381	9128.425
5	KP150C	Abrasive paper 150#	5.231	9300.140
	KP320AC	Abrasive paper 320#	4.572	10636.50
	KP600AC	Abrasive paper 600#	4.716	10312.593
	KP1000AC	Abrasive paper 1000#	4.787	10160.066
	KP1500AC	Abrasive paper 1500#	4.813	10105.34
	KS40C	Scalpel blade 40 μm	4.951	9824.48

Table 3 continued

Run no.	Temperature sensor no.	Scratch technique	$T_{TS} - T_{\infty}$ (K)	β_{TS} $\left(J \cdot m^{-2} \cdot K^{-1} \cdot s^{-1/2}\right)$
	KS60A	Scalpel blade 60 μm	4.36	11152.277
	KS60C	Scalpel blade 60 μm	5.276	9221.063
6	KP150C	Abrasive paper 150#	9.532	9706.94
	KP320AC	Abrasive paper 320#	7.641	12099.46
	KP600AC	Abrasive paper 600#	7.561	12227.055
	KP1000AC	Abrasive paper 1000#	7.741	11943.660
	KP1500AC	Abrasive paper 1500#	8.283	11164.71
	KS40C	Scalpel blade 40 μm	9.621	9617.51
	KS60A	Scalpel blade 60 μm	8.177	11308.93
	KS60C	Scalpel blade 60 μm	9.781	9460.83

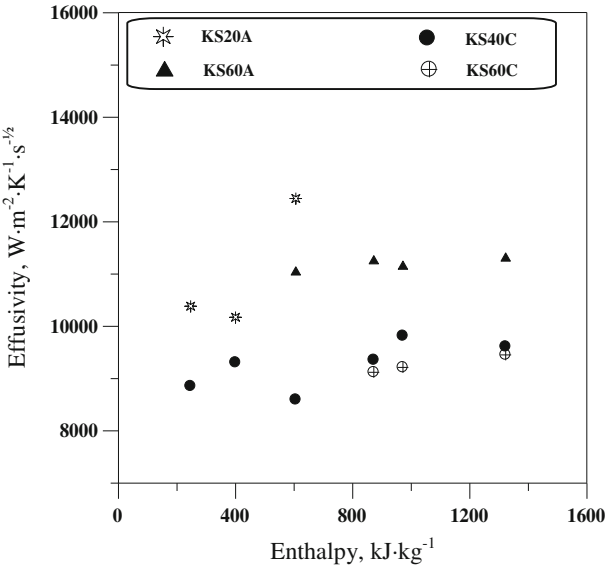

Fig. 8 Effusivity versus enthalpy for different temperature sensors scratched using scalpel blade

helium–CO_2 combination were then combined with the effusivity for $CO_2(\beta_{R5})$ to deduce the effusivity for the fabricated temperature sensors.

5.2.1 Scalpel Blade Scratch Technique

For the experiments where the sensor junction was formed by the scalpel blade scratch technique, the effusivity values for each run are plotted in Fig. 8. It was observed that when the junction was formed on the alumel element, the mean values of the effusivity

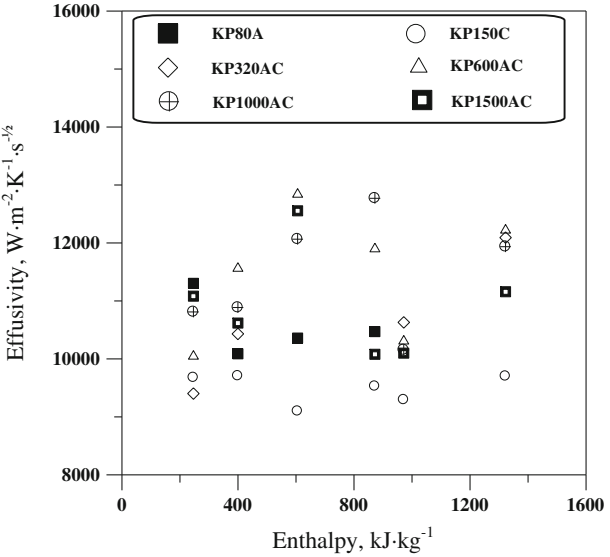

Fig. 9 Effusivity versus enthalpy for different temperature sensors scratched using abrasive paper

for the test runs produced from KS20A and KS60A varied between 11 009.26 $\mathrm{J \cdot m^{-2} \cdot K^{-1} \cdot s^{-1/2}}$ and 11 190.01 $\mathrm{J \cdot m^{-2} \cdot K^{-1} \cdot s^{-1/2}}$. These effusivity values correspond closely to that of alumel identified from the correlation equations developed earlier. However, when the junction was formed on the chromel element, the mean values of the effusivity for the test runs produced from KS40C and KS60C varied between 9 264.02 $\mathrm{J \cdot m^{-2} \cdot K^{-1} \cdot s^{-1/2}}$ and 9 270.11 $\mathrm{J \cdot m^{-2} \cdot K^{-1} \cdot s^{-1/2}}$. Both of these values are closer to each other and are higher than the correlated value for chromel identified from the developed correlation equations. It is worth mentioning that the derivation of the effusivity from the measured data is slightly more sensitive to the temperature difference $(T_{\mathrm{Ts}} - T_{\infty})$ than it is to the effusivity of CO_2. Thus, the uncertainty in $(T_{\mathrm{Ts}} - T_{\infty})$ is estimated to be 1.2 % and the estimated uncertainty in the sensor effusivity is approximately 2.8 % with the strongest contribution from the uncertainty in the effusivity of CO_2. This level of uncertainty may consequently contribute to the differences in the measured and correlated chromel values. Furthermore, another factor needs to be considered which is that the temperature sensor is actually composed of three different materials that contribute to the effusivity value as has been demonstrated by the same authors in [21]. Furthermore, it seems that some of the junctions are located in the area close to the alumel element, and others are located in the proximity of the electrical insulation area. Therefore, the difference between the effusivity values for the junctions formed using the scalpel blade scratch technique onto alumel and chromel elements remains consistent for all of the scalpel scratched junctions tested. These results may suggest that it is not necessary to calibrate each temperature sensor to determine its effusivity value. Therefore, based on the present results, the effusivity for the sensor whose junction formed on the alumel element can be taken as 11 099.64 $\mathrm{J \cdot m^{-2} \cdot K^{-1} \cdot s^{-1/2}}$ with 95 % confidence limits of 4.18 %. The

effusivity can be taken as 9 267.06 $\mathrm{J \cdot m^{-2} \cdot K^{-1} \cdot s^{-1/2}}$ with 95 % confidence limits of 1.82 % for the sensor whose junction formed on the chromel element.

5.2.2 Abrasive Paper Scratch Technique

For the experiments where the sensor junction was formed by the abrasive paper scratch technique, the effusivity values for each run are plotted in Fig. 9. For sensors scratched using coarser grit size of abrasive paper (e.g., KP80A) from the chromel element onto the alumel element. In this case, multiple junctions were created by carefully drawing a small area of the grit size of abrasive paper from the chromel element onto the alumel element, and all localized junctions were created on the alumel element. Thus, the average value of the effusivity is 10 561.56 $\mathrm{J \cdot m^{-2} \cdot K^{-1} \cdot s^{-1/2}}$ which is obviously lower than the value of the effusivity of the sensor scratched using a scalpel blade (i.e., KS20A and KS60A). When the sensor junction was formed using a much finer grit size scratch such as KP600AC, KP1000AC, and KP1500AC, the effective locations of the sensor junctions are much closer to the insulation layer than when the scalpel blade was used to create the junctions. In this case, a relatively large area of abrasive paper is drawn across the entire face of the temperature sensor; therefore, the junctions are likely to be created on both alumel and chromel elements. The number of junctions on each element of the temperature sensor may not be equal, so it is possible that the effusivity of one of the element materials may dominate. In addition, the thermophysical properties of the insulation layer have a stronger influence on the effective values of the effusivity when finer junctions are created with abrasive paper. Thus, the mean values of effusivity of the above three sensors can be taken as 11 289.02 $\mathrm{J \cdot m^{-2} \cdot K^{-1} \cdot s^{-1/2}}$ with 95 % confidence limits of 6.32 % even though there are small variations in the values as shown in Fig. 9. The observed variations in the effusivity values is probably due to: (i) the differences of the thermophysical properties of the two sensor element materials coupled with the uncertain weighting for each; and (ii) the differences in the proximity of the junction to the insulation layer due to construction variability.

6 Uncertainty Analysis

The repeatability of the experimental results was grouped into two categories: (i) repeating a particular experiment under the same operating conditions, and (ii) repeating a particular temperature sensor design and fabrication using the same materials and using the same scratch technique such as KP80A/R* and KP150C/R* (Table 1) to check their repeated response. The repeatability of the measurements for each type of temperature sensor was within 5 %. In addition, the repeatability of the shock-tube calibration technique was also assessed using data from test runs 1 to 6 (Table 2) which were essentially repeated experiments with the same configuration. Considering the data for KP80A/R*, these runs produced a mean value of $\beta_{\mathrm{Al}} = 11\,748.63\,\mathrm{J \cdot m^{-2} \cdot K^{-1} \cdot s^{-1/2}}$ with a standard deviation of 5.02 %. This level of variability is significantly higher than the estimated uncertainty which indicates that the strongest contributions to the calculated values of $(T_{\mathrm{Ts}} - T_{\infty})$ are from the measured shock speed (uncertainty

of 0.5 %) and the thermal conductivity of CO_2 (uncertainty of 2 %), yielding a total uncertainty of 2.5 %. The difference between the duplicated experimental test runs was within 2 %.

Therefore, the overall uncertainty was estimated for all test runs and for all values of the driver pressure (P_4), driven pressure (P_1), shock wave speed (u), reflected wave speed (U_R), and surface temperature ($T_{Ts} - T_\infty$) using the method outlined in [33] and [34]. It was found, from the experiments conducted in this work, that the overall uncertainty for the static and dynamic pressure measurements arising from the calibration uncertainty is around 2 %, the scatter due to run-to-run variations is about 2 %, the amplifier and sampling uncertainty (both 1 %), and errors in the baseline pressure (2 %) for static pressure (negligible for dynamic pressure), giving overall uncertainties of approximately 5 % for static pressure and 3 % for dynamic pressure. The uncertainty in the heat flux arises from the uncertainty in the thermophysical properties of the temperature sensor elements (4 %), in the thermo-resistive properties of the elements (2 %), scatter due to run-to-run variations (2 %), and amplifier and sampling uncertainty (both 1 %), giving an overall uncertainty of approximately 5 %.

7 Conclusions

An experimental method using a transient shock-tube facility with different operating conditions was conducted to evaluate the effusivity values for in-house different scratched temperature sensors. The performance of these sensors was also discussed in this paper. The conclusions from this work can be summarized as follows:

1. Useful and practical data of effusivity values of different scratched temperature sensors were provided. These data are helpful to experimentalists in the field and can be used for accurate transient heat transfer rates.
2. The temperature sensor performance is significantly influenced by the method of forming the surface junction which in turn affects the effusivity value. New correlation equations for evaluating the thermophysical properties of the temperature sensor were derived.
3. There was a tendency for the effusivity of the temperature sensor to be different when it is formed using different scratch techniques. An accurate effusivity value of a particular temperature sensor depends upon whether the junction was actually located on the positive or negative element or on both and on its proximity to the thin insulating layer between the two elements.
4. The effusivity of a particular temperature sensor depends on the Mach number, scratch technique, scratch direction, and junction location, as well as on the enthalpy conditions.
5. It was observed that the fabricated temperature sensor using the scalpel blade technique does not require an individual calibration. However, a calibration for each temperature sensor whose junction was created using the abrasive paper technique is likely to be needed.
6. There are significant differences between the effusivity for junctions formed on the chromel element and those formed on the alumel element using the scalpel

blade technique. It was observed that the effusivity for alumel is larger than that of chromel by approximately 17 %.

References

1. A.C. Alkidas, J. Heat Transf. Trans. ASME **102**, 189 (1980)
2. A.C. Alkidas, R.M. Cole, J. Heat Transf. Trans. ASME **107**, 439 (1985)
3. A.C. Alkidas, P.V. Puzinauskas, R.C. Peterson, SAE Trans. J. Engines **99**, 817 (1990)
4. J.A. Gatowski, M.K. Smith, A.C. Alkidas, Exp. Therm. Fluid Sci. **2**, 280 (1989)
5. B. Lawton, J. Power Energy **201**, 175 (1987)
6. D.J. Oude Nijeweme, J.B.W. Kok, C.R. Stone, L. Wyszynski, J. Automob. Eng. **215**, 747 (2001)
7. C. Jessen, M. Vetter, H. Gronig, Z. Flugwiss Weltraumforsch **17**, 73 (1993)
8. S.L. Gai, W.S. Joe, J. Thermophys. Heat Transf. **6**, 433 (1992)
9. S.R. Sanderson, B. Sturtevant, Rev. Sci. Instrum. **73**, 2781 (2002)
10. B. Lawton, G. Klingenberg, *Transient Temperature in Engineering and Science* (Oxford University Press, Oxford, 1996)
11. J.C. Chen, K.K. Hsu, J. Heat Transf. Trans. ASME **117**, 693 (1995)
12. L. Lee, J.C. Chen, R.A. Nelson, Rev. Sci. Instrum. **53**, 1472 (1982)
13. L.Y.W. Lee, J.C. Chen, R.A. Nelson, J. Heat Mass Transf. **28**, 1415 (1985)
14. D. Bendersky, Mech. Eng. **75**, 117 (1953)
15. A. Kovas, R.B. Mesler, Rev. Sci. Instrum. **35**, 485 (1964)
16. L. Ongkiehong, J. Van Dujin, J. Sci. Instrum. **37**, 221 (1960)
17. NANMAC, *Temperature Measurement Handbook*, vol. VIII (Nanmac Co. Publication, Framingham, MA, 1997)
18. H. Mohammed, H. Salleh, M.Z. Yusoff, Int. Commun. Heat Mass Transf. **35**, 853 (2008)
19. P.A. Kinzie, *Thermocouple Temperature Measurement* (Wiley, New York, 1973)
20. K. Raznjevic, *Handbook of Thermodynamics Tables and Charts* (McGraw Hill, New York, 1976)
21. H. Mohammed, H. Salleh, M.Z. Yusoff, Therm. Sci. **11**, 49 (2007)
22. D.R. Buttsworth, Exp. Therm. Fluid Sci. **25**, 409 (2001)
23. Y. Heichal, S. Chandra, E. Bordatchev, Exp. Therm. Fluid Sci. **30**, 153 (2005)
24. T. Sprinks, AIAA J. **1**, 464 (1963)
25. P.R.A. Lyons, S.L. Gai, J. Phys. E: Sci. Instrum. **21**, 445 (1998)
26. F.R. Caldwell, *Applied Methods and Instrument; Temperature: Its Measurement and Control in Science and Industry*, vol. 3, part 2 (Reinhold, New York, 1962), pp. 81–134
27. Y.S. Touloukian, *Thermophysical Properties of Matter; Temperature Sensor RC Data Series*, vol. 4 (IFI/Plenum Press, New York, 1970)
28. Y.S. Touloukian, *Thermophysical Properties of Matter; Temperature Sensor RC Data Series*, vol. 1 (IFI/Plenum Press, New York, 1970)
29. J.D. Anderson, *Modern Compressible Flow with Historical Perspective*, 3rd edn. (McGraw Hill, New York, 2004)
30. M.J. Zurcow, J.D. Hoffman, *Gas Dynamics* (Wiley, New York, 1976)
31. F.M. White, *Viscous Fluid Flow*, 2nd edn. (McGraw Hill, New York, 1991)
32. N.B. Vargaftik, Y.K. Vinogradov, V.S. Yargin, *Handbook of Physical Properties of Liquids and Gases*, 3rd edn. (Begell House, New York, 1996)
33. H.W. Coleman, W.G. Steele, AIAA J. **33**, 1888 (1995)
34. N.C. Baines, D.J. Mee, M.L.G. Oldfield, Int. J. Eng. Fluid Mech. **4**, 375 (1991)